This paper appears in Mechatronics, 2022.
https://doi.org/10.1016/j.mechatronics.2022.102821

Intelligent Assistance for Older Adults via an Admittance-Controlled Wheeled Mobile Manipulator with Task-Dependent End-Effectors

Liang Ding[a], Hongjun Xing[a,b,*], Ali Torabi[b], Javad K. Mehr[b,c], Mojtaba Sharifi[b,c,d], Haibo Gao[a], Vivian K. Mushahwar[c], Mahdi Tavakoli[b,*]

[a]*State Key Laboratory of Robotics and System, Harbin Institute of Technology, Harbin 150001, China*
[b]*Department of Electrical and Computer Engineering, University of Alberta, Edmonton T6G 1H9, Alberta, Canada*
[c]*Department of Medicine, Division of Physical Medicine and Rehabilitation, University of Alberta, Edmonton T6G 2E1, Alberta, Canada*
[d]*Department of Mechanical Engineering, Charles W. Davidson College of Engineering, San Jose State University, San Jose, CA 95192-0087, USA*

Abstract

The increase in the ageing population worldwide poses a severe challenge in assisting older individuals to live independently, including the provision of mobility assistance and support in daily activities. In this paper, a practical robotic system is developed to provide intelligent support for older persons using a wheeled mobile manipulator (WMM), consisting of an omnidirectional mobile platform and a robotic arm. We focus on two critical needs: 1) mobility assistance, and 2) object manipulation support. The tasks are not executed simultaneously and each uses a task-dependent end-effector. Learning from demonstration, or kinesthetic teaching, is adopted to help the WMM to learn an elderly or disabled user's walking pattern or an able-bodied person's object manipulation skill. The robotic system can assist the user in conducting a number of daily operations. For mobility assistance, the WMM is reconfigured into a smart walker, where a novel variable admittance control is adopted to detect the user's walking intention. A learning approach based on dynamic movement primitives is implemented to capture and adapt the WMM to the user's walking pattern. For object manipulation support, a demonstrator first collaborates with an elderly user to conduct the task, and then the WMM takes the role of the demonstrator to assist the user. The Gaussian mixture model and Gaussian mixture regression are used to learn and reproduce the demonstrator's experience, respectively. The advantages and effectiveness of the proposed approach are experimentally demonstrated with a four-wheel omnidirectional WMM.

Keywords: Wheeled mobile manipulator (WMM), mobility assistance, human-robot collaboration (HRC), compliance control, learning from demonstration (LfD).

1. Introduction

Seniors or adults with chronic conditions who have motor disabilities often use assistive devices to walk and to perform activities of daily living [1, 2]. The desirable movement capability of mobile robots is drawing a lot of attention [3], especially wheeled mobile manipulator (WMM)-based assistive devices that are widely studied and used due to their desirable movement capability on flat ground as well as their operational capability [4, 5, 6]. Employing a robotic assistance system may reduce the dependence on caregivers, reduce costs of health care, and ensure timely support during the performance of activities of daily living [7]. Moreover, due to the impact of the COVID-19 pandemic, robotic assistance devices have found many applications as a means of reducing the chances of infection of their users [8]. However, the traditional assistive equipment has some drawbacks, including the need for considerable forces to activate the devices and the lack of adaptation to the user's motion. A practical robotic system is urgently needed to assist older persons in their daily lives by conducting multiple daily tasks.

Muscle weakness, joint stiffness, and physical impairments often experienced by older adults make their independent living needs challenging. Implementing a robotic assistance system may be able to address these needs [9]. Two major kinds of applications can be considered. One is to rely on the robot to serve the user completely, such as robotic clothing assistance and cup fetching [10, 11]. The other is to view the robot as a collaborator to cooperate with the user to accomplish various tasks such as moving a table or furniture [12, 13]. The latter is more complicated than the former since it requires taking the human-robot interaction (HRI) into account, which is one of the main foci of the work described in this study. Mobility assistance and human-robot collaboration (HRC) for object manipulation are two everyday tasks in the daily life of older adults; thus, they are selected as the targets for robotic assistance to be provided via one WMM.

Two commonly utilized devices for mobility assistance are robotic canes (single-hand operation) and intelligent walkers

*Corresponding authors
Email addresses: liangding@hit.edu.cn (Liang Ding), xinghj@hit.edu.cn (Hongjun Xing), ali.torabi@ualberta.ca (Ali Torabi), j.khodaeimehr@ualberta.ca (Javad K. Mehr), mojtaba.sharifi@sjsu.edu (Mojtaba Sharifi), gaohaibo@hit.edu.cn (Haibo Gao), vivian.mushahwar@ualberta.ca (Vivian K. Mushahwar), mahdi.tavakoli@ualberta.ca (Mahdi Tavakoli)

(dual-hand operation) [6, 14]. Most of the mobility assistance-related work has focused on developing novel compliant interaction approaches (considering user-applied horizontal interaction forces) to ensure user safety and improve their experience. Examples include variable admittance control (VAC) and adaptive impedance control, which may also integrate modern learning techniques to train the control parameters [15].

The deployment of mobile manipulators in HRC has attracted many researchers in recent years [13, 16, 17, 18]. The exploitation of WMMs can ease the kinematic and dynamic limitations of robotic systems. For instance, the WMM has an unlimited workspace in the horizontal plane. Also, redundancy in the WMM system (availability of more degrees of freedom than the task minimally needs) can enhance some required features for a task with null-space control [19].

The challenge for an intelligent assistance device is learning and adapting to the user's motion pattern. Learning-based approaches have the advantage of intuitively transferring a human's knowledge of how to perform a task to a robot using methods such as Gaussian mixture regression (GMR) and Gaussian process regression (GPR) [12]. Gaussian mixture model (GMM) combined with GMR can provide additional motion information for robots while they are learning from multiple demonstrations compared with other learning methods [20]. Dynamic movement primitives (DMPs) have also found many applications, especially in learning a trajectory where human-robot interaction forces are considered [21]. DMPs use a single demonstration, have spatial and temporal scalability and can guarantee convergence to a goal position, giving DMPs an advantage over methods based on statistical machine learning [22].

This paper aims to provide an intelligent assistance system employing a WMM with task-appropriate end-effectors to tackle mobility assistance and object co-manipulation. The two tasks are accomplished separately by the WMM with a task-dependent end-effector. Although some problems are still unsolved, such as how to exchange the end-effectors automatically, this paper provides a beneficial attempt to facilitate older persons' lives by helping them conduct multiple tasks with one robotic device.

The main contributions of the paper are as follows: (1) A robotic system employing a WMM to assist older adults in conducting multiple daily activities with task-dependent end-effectors is proposed; (2) for mobility assistance, an intelligent strategy is developed to learn any user-specified walking pattern over one gait cycle by employing novel cooperative DMPs for mobility assistance, where a novel VAC approach is designed to detect and respond to the user's intention and the coupled term in the proposed cooperative DMPs is implemented to handle emergency conditions (*e.g.*, large unintended force or fall); (3) for heavy object manipulation support, a stiffness estimation method and a GMR technique, based on GMM, are adopted to reproduce the user's impedance-based behavior in the vertical direction, and realize the compliant motion demand in the horizontal plane, respectively. A configuration optimization approach is provided to enhance the WMM's force exertion capability in a predefined direction to deal with heavy loads.

The remainder of this paper is organized as follows. State of the art and open challenges of intelligent assistance are described in Section 2. Section 3 presents a motivation demonstration of this research. Section 4 provides the kinematic modeling and admittance control-based control scheme for the WMM. In Section 5, the locomotion pattern learning and personalization methods for mobility assistance via the proposed cooperative DMPs are presented. In Section 6, the learning and reproduction approaches from human demonstration for HRC are illustrated. Experiments that illustrate the validity and advantages of the proposed approach are shown in Section 7. Section 8 summarizes the approach and its outcomes.

2. Related Work

Intelligent assistance devices are commonly designed to provide support for one specific task [23]. A common example is the walker, historical overviews of smart walkers are available in [1, 14, 24]. The primary focus in this area has been on designing more user-friendly interaction compliance approaches, considering only the user-applied horizontal forces as an indication of the user's intention to move in a particular direction [5, 25]. The FriWalk robotic walker, developed by the EU Research project ACANTO, provided the user with several physical and cognitive support options for navigation in a complex environment [26, 27]. The FriWalk had solid sensing and computing capabilities to generate suitable trajectories for the user. Moreover, practical functions, such as obstacle avoidance and corridor following, were also incorporated [28].

Jiménez *et al.* [29] presented an admittance controller for a smart walker, which could generate haptic signals to help the tracking of a predetermined path. When deviating from the path, the walker adjusted the user's direction by varying the damping parameter of the controller through a spatial modulation technique. Itadera *et al.* [5] designed a robotic assistive device with an admittance controlled mobile base to provide walking assistance for older adults through predictive optimization of gait assistive force. An optimization algorithm based on a model predictive control approach was presented to offer desirable assistive forces to reduce the risk associated with immobility, such as disuse syndrome. Despite the extensive work in this area, to the best of our knowledge, incorporation of the vertical interaction between the user and the mobility assistance device to better detect the user's intention has not been investigated, nor has the use of learning-based approaches to learn the user's walking pattern for personalizing the assistance to the user. These two approaches are addressed in this paper.

In terms of object manipulation through HRC, the challenge is in the system's understanding of the user's intention. This, however, can be addressed through learning from demonstration (LfD) by intuitively transferring a human's knowledge of a task to a robot through demonstrations [30]. Fong *et al.* [7] utilized GMM and GMR to learn an object lifting motion with rehabilitation robots. Rozo *et al.*[12] put forward a task-parameterized version of GMM (TP-GMM) to encode the demonstrations, and used GMR to reproduce the learned

results. This method has been effectively implemented in HRC transportation and assembly missions.

Al-Yacoub *et al.* [31] presented an LfD approach for object co-manipulation that combined a machine learning algorithm – *i.e.*, Random Forest – with stochastic regression, using haptic information captured from human demonstration. Gienger *et al.* [32] provided a system for cooperatively manipulating large objects between a human and a robot, which was able to handle, transport, or manipulate large objects of different shapes in cooperation with a human, even including contact changes. More overviews investigating HRC issues can be found in [33, 34].

To date, the existing research has only focused on one single portion of the mission, such as moving an object [12] and handing over an object [35]. Moreover, previous work has not addressed the problem of the robotic system's limited force exertion capability for heavy object manipulation, which may be a limitation for a robot to assist the user in conducting collaboration tasks. These are aspects that are investigated in this study.

3. Main Concept and Approach

In the existing mobility assistance devices, the users commonly need to apply an adequate horizontal force to activate them. These devices are mostly not "smart" enough to detect how to respond to the users' walking pattern [5, 36]. Fig. 1 presents a general diagram of human mobility assistance with a WMM. The robot only bears a vertical force (f_z) from the user at the start state (Fig. 1a). When the user wants to move towards a direction, they will apply a considerable horizontal force (f_x) in the direction indicating their walking intention (Fig. 1b). The user then generates a small horizontal force as they continue their motion (Fig. 1c). Here, we consider both the user-applied horizontal and vertical force components to detect the user's locomotion intention. A large vertical force applied by the user causes a small horizontal motion to achieve better support. An LfD technique is employed to learn the users' walking pattern to improve their comfort and reduce their energy expenditure.

An HRC for object manipulation with a WMM is presented as an example to illustrate robotic assistance in completing daily tasks; part of this work has been presented in [37]. With the WMM support, the user can complete some tasks with less energy. Fig. 2 shows the general diagram of manipulating an object using LfD, which can be divided into three steps: lifting, carrying, and lowering. Fig. 2a shows the demonstration phase, where a demonstrator/helper teaches the WMM how to handle the task with the user. The WMM then learns the demonstrator's task skills and completes the task independently with the user, as shown in Fig. 2b. The lifting and lowering steps contain considerable force output in the vertical direction during movement. Thus, the interaction force between the human and the object should be learned in addition to the motion between them. The carrying step involves only the desirable compliant movement in the horizontal plane. Therefore, only the kinematic motion is learned and reproduced. This is, to the best of our knowledge, the first time the LfD technique is implemented to imitate the human's action for an object manipulation task considering all three steps [12, 38].

4. Kinematics and Compliance Control of WMMs

In this section, the forward kinematics at the velocity level for WMMs are presented. A task-space admittance control scheme to achieve compliance and a null-space optimization algorithm to realize force exertion capability enhancement are also provided.

4.1. Kinematics of WMMs

The kinematic model of a mobile platform without slippage or skidding can be expressed as $\dot{q}_p = G(q_p)v_p$, where $\dot{q}_p \in \mathbb{R}^{n_p}$ represents the generalized coordinate vector of the mobile platform and $v_p \in \mathbb{R}^p$ is the input velocity vector of the wheels. $G(q_p) \in \mathbb{R}^{n_p \times p}$ denotes the constraint matrix of the platform (holonomic or nonholonomic). The generalized velocity vector of the manipulator $\dot{q}_m \in \mathbb{R}^m$ can be assigned arbitrarily at any manipulator configuration. Here, we specify $\dot{q}_m = v_m$, where $v_m \in \mathbb{R}^m$ denotes the joint velocity input vector for the manipulator.

The generalized coordinate vector and velocity input vector of the WMM are defined as $q = [q_p^{\mathrm{T}}, q_m^{\mathrm{T}}]^{\mathrm{T}} \in \mathbb{R}^{n_p+m}$ and $v = [v_p^{\mathrm{T}}, v_m^{\mathrm{T}}]^{\mathrm{T}} \in \mathbb{R}^n$, respectively, where $n = p+m$. Then, its forward kinematics at velocity level can be calculated as

$$\dot{x} = \begin{bmatrix} J_p(q), J_m(q) \end{bmatrix} \begin{bmatrix} \dot{q}_p \\ \dot{q}_m \end{bmatrix} = \begin{bmatrix} J_b(q)G(q_p), J_m(q) \end{bmatrix} \begin{bmatrix} v_p \\ v_m \end{bmatrix} = J(q)v, \tag{1}$$

where $\dot{x} \in \mathbb{R}^r$ is the task-space velocity vector of the end-effector in the world frame Σ_w with its dimension being r, $J_p(q) \in \mathbb{R}^{r \times n_p}$ and $J_m(q) \in \mathbb{R}^{r \times m}$ denote the Jacobians of the mobile platform and the manipulator, respectively, and $J(q) \in \mathbb{R}^{r \times n}$ represents the Jacobian of the WMM.

Then, with the WMM velocity vector defined as v, the inverse kinematics of the WMM can be expressed as

$$v = J^{\dagger}\dot{x}, \tag{2}$$

where $J^{\dagger} = WJ^{\mathrm{T}}(JWJ^{\mathrm{T}})^{-1}$ is the weighted pseudoinverse of J with $W \in \mathbb{R}^{n \times n}$ being a symmetric and positive-definite weighting matrix.

4.2. Compliance Rendered by an Admittance-Based Control Scheme

To achieve robot learning by human demonstration, the WMM should be compliant with the human or environment's external force. Thus, an admittance control scheme is adopted here with the transfer function at velocity level expressed as

$$\frac{\dot{x}_f(s)}{f_h(s)} = G(s) = \frac{s}{\Lambda s^2 + \Upsilon s + \Gamma}, \tag{3}$$

where s denotes the Laplace operator, $f_h \in \mathbb{R}^r$ denotes the user-applied force vector, and $\dot{x}_f \in \mathbb{R}^r$ represents the resultant end-effector velocity vector. $\Lambda \in \mathbb{R}^{r \times r}$, $\Upsilon \in \mathbb{R}^{r \times r}$, and $\Gamma \in \mathbb{R}^{r \times r}$ are

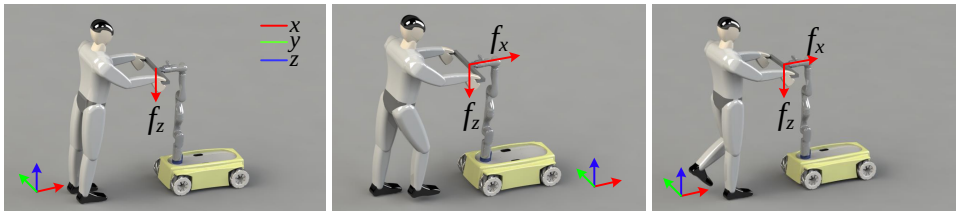

(a) Initial state (b) Motion with a big force (c) Motion with a small force

Figure 1: Illustration of mobility assistance with a WMM.

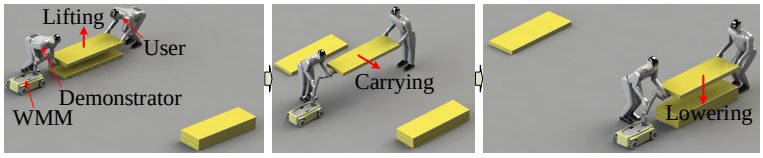

(a) Human demonstration

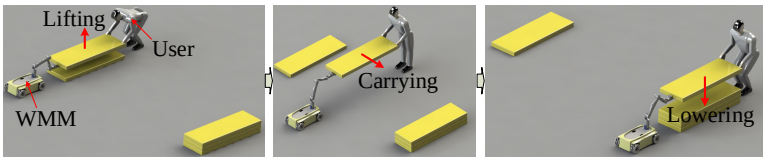

(b) Robot imitation

Figure 2: Illustration of LfD procedure for object manipulation via HRC.

diagonal matrices representing the desired task-space inertial, damping, and stiffness, respectively.

The admittance controller (3) is designed to achieve compliance in any r-dimensional space, which is not suitable for a mobility assistance device since the vertical motion is not required. A novel admittance controller is proposed to detect the user's walking intention, and the WMM for mobility assistance is also called a smart walker thereafter. Unlike the previous research considering only the horizontal forces [39], we also include the vertical force to detect the user's intention. The smart walker here is programmed to slow down when the user applies a large vertical force. A large vertical force aims to simulate the user's falling incident. When the user uses a large horizontal force, the robotic walker is controlled to speed up to provide mobility assistance.

To further improve the performance of mobility assistance, a custom-built variable admittance controller for the walker is designed as

$$\begin{bmatrix} \dot{x}_{fx} \\ \dot{x}_{fy} \\ \dot{x}_{tz} \end{bmatrix} = \begin{bmatrix} G_{xx} & 0 & G_{xz} & 0 \\ 0 & G_{yy} & G_{yz} & 0 \\ 0 & 0 & 0 & G_{zz} \end{bmatrix} \begin{bmatrix} f_x \\ f_y \\ f_z \\ \tau_z \end{bmatrix} \tag{4}$$

with

$$G_{ii} = \frac{1}{\Lambda_i s + \Upsilon_i}, \; G_{jz} = \frac{-1}{\Lambda_{jz} s + \Upsilon_{jz}} \text{sign}(f_j),$$

where $i \in \{x, y, z\}$, $j \in \{x, y\}$. $\dot{x}_{fx}$, $\dot{x}_{fy}$, and $\dot{x}_{tz}$ represent the velocity component of $\dot{x}_f$ caused by the user-applied wrench. τ_z denotes the user's z direction torque, and f_x, f_y, and f_z denote the user's interaction forces in x, y, and z directions, respectively. Λ_{jz} and Υ_{jz} represent the desired constant inertial and damping, which relate the vertical force (f_z) with the horizontal velocities ($\dot{x}_{fx}$ and $\dot{x}_{fy}$). This scheme reduces the walker's horizontal motion when a large vertical force is exerted. Λ_i and Υ_i are the desired variable inertial and damping relating the user's wrench with its corresponding velocity/angular velocity, which is expressed as

$$\begin{cases} \Upsilon_x(f_x) = \Upsilon_{x0} - \alpha |f_x|, \; \Lambda_x = \frac{\Lambda_{x0}\Upsilon_x(f_x)}{\Upsilon_{x0}}, \\ \Upsilon_y(f_y) = \Upsilon_{y0} - \beta \left|f_y\right|, \; \Lambda_y = \frac{\Lambda_{y0}\Upsilon_y(f_y)}{\Upsilon_{y0}}, \\ \Upsilon_z(\tau_z) = \Upsilon_{z0} - \gamma |\tau_z|, \; \Lambda_z = \frac{\Lambda_{z0}\Upsilon_z(\tau_z)}{\Upsilon_{z0}}. \end{cases} \tag{5}$$

Here, α, β, and γ are positive gains. Eq. (5) tries to decrease the damping of the walker to make it move faster when a significant force or torque is applied in the corresponding direction and maintains the stability of the control system by keeping the ratio between the inertia and the damping.

4.3. Null-Space Control Scheme to Realize Force Enhancement

For a reference end-effector velocity vector defined as $\dot{x}_r(t)$, unlike (2), the kinematic controller of a redundant WMM with null-space control considered can be expressed as

$$v_r = J^{\dagger}\dot{x}_r + (I - J^{\dagger}J)v_N, \tag{6}$$

where $v_r \in \mathbb{R}^n$ represents the reference WMM's joint velocity vector, I represents an $n \times n$ identity matrix, $I - J^{\dagger}J$ is the null-space of J, and $v_N \in \mathbb{R}^n$ is the null-space velocity vector for configuration optimization.

For heavy object manipulation tasks via HRC, the required force to counteract the object weight may be large. Due to

the limited manipulator joint torque output, some heavy objects cannot be lifted. Hence, the null-space control is implemented to enhance the end-effector's force exertion capability via kinematic reconfiguration.

A scalar cost function is defined as

$$\sigma_1 = \left[u^{\mathrm{T}}(J_m W_\tau W_\tau J_m^{\mathrm{T}})u\right]^{-1} \tag{7}$$

to maximize the end-effector's force exertion ability in the predefined direction, where $u \in \mathbb{R}^r$ is a unit vector denoting the optimization direction. $W_\tau = \mathrm{diag}\left[\frac{1}{\tau_{m\lim_1}} \cdots \frac{1}{\tau_{m\lim_m}}\right]$ denotes a scaling matrix to normalize the joint torques with $\tau_{m\lim_i}$ being the torque limit of the i^{th} joint. To eliminate the influence of manipulator's gravity, another cost function is specified as

$$\sigma_2 = f_g^{\mathrm{T}} f_g / \varrho, \tag{8}$$

where $f_g = J_m^{-\mathrm{T}}\tau_g$ with $\tau_g \in \mathbb{R}^m$ being the joint torque vector caused by the manipulator gravity and ϱ is a positive scalar gain, which makes targets σ_1 and σ_2 on the same order of magnitude. Combining (7) and (8), the cost function for the null-space controller can be defined as $\sigma = w_1\sigma_1 - w_2\sigma_2$, where w_1 and w_2 are two constant gains with $w_1 + w_2 = 1$. By calculating the partial derivative of σ to q_m, denoting as $\nabla_{q_m}\sigma$, we can obtain the null-space joint velocity vector for (6) as

$$v_N = k_N \begin{bmatrix} 0_{p\times 1} \\ (\nabla_{q_m}\sigma)^{\mathrm{T}} \end{bmatrix} \tag{9}$$

with k_N being a constant gain.

5. Locomotion Pattern Learning and Personalization via Cooperative DMPs

In this section, the proposed cooperative DMPs to learn the human's walking pattern will be presented. Section 5.1 introduces the concept of the proposed method. Section 5.2 illustrates how to train the learning system. Implementing the method for assisting bipedal mobility is presented in Section 5.3.

5.1. Cooperative Dynamic Movement Primitives

The classical DMPs were first proposed by Ijspeert *et al.* [21], which can be divided into two categories, one is discrete DMPs for point-to-point motions, and the other is rhythmic DMPs for periodical patterns. For point-to-point movement, which is suitable for this research, the discrete DMPs can be written as [21]

$$\tau\dot{n} = \alpha_n(\beta_n(g - m) - n) + f(\kappa), \tag{10}$$

$$\tau\dot{m} = n, \tag{11}$$

$$\tau\dot{\kappa} = -\alpha_\kappa\kappa, \tag{12}$$

and forcing the term $f(\kappa)$ to be a linear combination of radial basis functions to learn the motion pattern

$$f(\kappa) = \frac{\sum_{i=1}^{N} w_i\Psi_i(\kappa)}{\sum_{i=1}^{N}\Psi_i(\kappa)}\kappa, \tag{13}$$

$$\Psi_i(\kappa) = \exp(-(\kappa - c_i)^2/(2\sigma_i^2)), \tag{14}$$

where $i = 1, 2, \cdots, N$ with N denoting the number of the basis functions, m denotes a single degree of freedom (DOF) trajectory, g denotes the attractor point of the trajectory, n and κ are two internal states, α_n, β_n, α_κ are three positive numbers, $\tau > 0$ determines the duration of the trajectory. w_i denotes the Gaussian kernel weights, which will be determined later. σ_i and c_i are constants to regulate the basis functions' widths and centers, respectively.

Equations (10) and (11) are the *transformation system*, (12) is the *canonical system*, and the phase variable κ is introduced to avoid dependence of $f(\kappa)$ on time. It is worth mentioning that $f(\kappa)$ in (10) will effectively vanish when g is reached to ensure the stability of the DMPs system. For a system with more than one DOF, the movement in each DOF will be represented with its own *transformation system*, and the entire robotic system will then be synchronized using the same *canonical system*.

The traditional DMPs (10)-(14) do not possess the ability to react to unpredictable events from the environment, but this is reasonably necessary for a smart walker controller. Fortunately, DMPs can be modulated online to incorporate a straightforward repulsive force to deal with emergencies [40]. Inspired by the concept of DMPs and [41], a cooperative DMPs used for mobility assistance in this paper are designed as

$$\tau\dot{n} = \alpha_n(\beta_n(g(\dot{x}_f) - m) - n) + f(\kappa) + \delta\dot{A}, \tag{15}$$

$$\tau\dot{m} = n + A, \tag{16}$$

$$g(\dot{x}_f) = \int_0^t (\dot{m}_{ave} + \dot{x}_f)\,\mathrm{d}\tau, \tag{17}$$

$$A = -\frac{1}{\eta(m_L - m)^3}, \tag{18}$$

$$\tau\dot{\kappa} = -\frac{\alpha_\kappa \exp[(\alpha_\kappa/\delta_t)(\tau T - t)]}{\{1 + \exp[(\alpha_\kappa/\delta_t)(\tau T - t)]\}^2}. \tag{19}$$

Here, (17) realizes the adaptation to the user intention, where $g(\dot{x}_f)$ is a dynamical attractor trajectory to guide the user's walking, $\dot{m}_{ave}$ represents the average user demonstration velocity in one gait and $\dot{x}_f$ denotes the velocity resulted from the VAC. The term A is added to circumvent the walker's motion by setting a manual limit m_L, where δ and η are two positive constants, and this term will only take effect when a big unintended force is applied (indicating the user's instability or falling). The sigmoidal decay equation (19) is selected instead of exponential decay equation (12) to avoid the rapid vanishment of $f(\kappa)$ [42], where δ_t is the sampling time and T is the duration of the trajectory. Here, the initial condition of κ is selected as $\kappa(0) = 1$.

The procedure of implementing this approach will be shown in Section 5.3 later.

5.2. Locomotion Learning from Demonstrated Walking Gait

The term $f(\kappa)$ in (13) is the crucial term to learn the user's walking pattern. The advantage is that $f(\kappa)$ is designed to be linear with respect to w_i, which allows us to use many methods to fit w_i.

Two phases are included in this framework. The learning phase learns the user's walking pattern, and the personalization

phase clones the learned walking skills and also adapts to the motion variations. During the learning phase, the walker is first activated employing an admittance controller to make it flexible enough for the user. Then, the walker's position, velocity, and acceleration are recorded (assuming they are the user's locomotion information) as the user pushes the admittance-controlled walker for trajectory learning. The term A in (18) is omitted and the attractor point $g(\dot{x}_f)$ in (17) is defined as the final point of the demonstrated trajectory to learn the user's normal walking pattern. It should be noted that only one gait of the user's motion will be learned; thus, the recorded data are cut into several bipedal walking gaits, and the average period of the gaits will also be identified.

After preprocessing the data obtained during the demonstration phase, the demonstrated user trajectory in one gait is denoted as $m_{demo}(t)$, where $t \in [1, 2, \cdots, P]^{\mathrm{T}}$ with $P = T_{demo}/\delta_t$ and T_{demo} representing the identified gait period. Its first time derivative and second time derivative are represented as $\dot{m}_{demo}(t)$ and $\ddot{m}_{demo}(t)$, respectively, and the attractor point in each cycle is g_{demo}. According to (15), the approximation of the term $f_{demo}(t)$ can be expressed as

$$f_{demo} = \tau^2 \ddot{m}_{demo} - \alpha_n(\beta_n(g_{demo} - m_{demo}) - \tau \dot{m}_{demo}). \tag{20}$$

Thus, the problem is reduced to implementing a method that makes $f(\kappa)$ as close as possible to $f_{demo}(t)$.

Here, Locally Weighted Regression (LWR) [41] is selected to update these weights w_i in (13). Collecting each $f_{demo}(t)$ and w_i into the vectors $\mathcal{F} = [f_{demo}(1), f_{demo}(2), \cdots, f_{demo}(P)]^{\mathrm{T}}$ and $\mathcal{W} = [w_1, w_2, \cdots, w_N]^{\mathrm{T}}$, one derives

$$\Phi \mathcal{W} = \mathcal{F} \tag{21}$$

with

$$\Phi = \begin{bmatrix} \frac{\Psi_1(\kappa_1)}{\sum_{i=1}^{N} \Psi_i(\kappa_1)} \kappa_1 & \cdots & \frac{\Psi_N(\kappa_1)}{\sum_{i=1}^{N} \Psi_i(\kappa_1)} \kappa_1 \\ \vdots & \ddots & \vdots \\ \frac{\Psi_1(\kappa_P)}{\sum_{i=1}^{N} \Psi_i(\kappa_P)} \kappa_P & \cdots & \frac{\Psi_N(\kappa_P)}{\sum_{i=1}^{N} \Psi_i(\kappa_P)} \kappa_P \end{bmatrix}.$$

Then, the weights vector $\mathcal{W}$ is updated in a least-square sense as

$$\mathcal{W} = (\Phi^{\mathrm{T}} \Phi)^{-1} \Phi^{\mathrm{T}} \mathcal{F}. \tag{22}$$

5.3. Locomotion Pattern Personalization with User Intention Considered

Unlike classical learning methods, wherein the reproduction phase the robotic system tries to reproduce the same trajectory it has learned [7], the locomotion pattern personalization phase in this paper regards the learned trajectory as an initial reference to assist the user's walking. For mobility assistance, the final position (attractor point) of a motion cannot be determined in advance; thus, only the walking pattern in one gait is learned, and it will be cloned cyclically in the personalization phase to adapt to variations.

Besides copying the learned motion, the attractor point in each gait $g(\dot{x}_f)$ will also be updated considering the interaction force-related motion $\dot{x}_f$ (determined in (4)). The circumvention term A will be added to stop the walker's motion when a large abnormal force is exerted (implying the user's possible falling or instability).

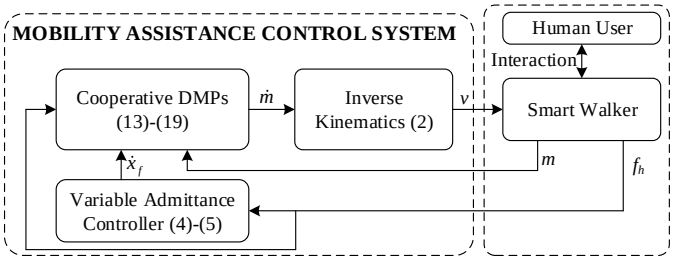

Figure 3: Block diagram of the mobility assistance control system.

Algorithm 1 Learning phase for mobility assistance via DMPs.

Prerequisite: τ, α_n, β_n, α_κ, c_i, σ_i, δ_t.

Steps:

1: Admittance control the walker to derive the normal user's walking trajectories including m_{demo}, $\dot{m}_{demo}$, and $\ddot{m}_{demo}$;
2: Manually divide the trajectories into several gaits, determine the average velocity of the gaits $\dot{m}_{ave}$ and find the gait period T_{demo};
3: Resample the preprocessed gait data with the same length P;
4: Calculate approximated $f_{demo}(t)$ via (20);
5: Develop vector $\mathcal{F}$ and matrix Φ via (21);
6: Derive and record weights vector $\mathcal{W}$ via (22).

The personalization phase is conducted as shown in (15)-(18) with the learned $f(\kappa)$ in (13)-(14). A control diagram of the proposed mobility assistance method is shown in Fig. 3, where the detailed learning and personalization phases are further explained in **Algorithm** 1 and **Algorithm** 2, respectively. In **Algorithm** 2, the forward walking motion in the x direction will be presented as an example to show the personalization approach. Here, **Steps** 2-6 are executed to ensure the learning system is activated only when the user interacts with the walker (indicating by an adequate vertical force); **Steps** 7-10 make sure the stable stopping of the walker when an emergency occurs (revealed via a considerable pushing force or vertical force).

6. Learning and Reproduction of Collaboration Skills from Human Demonstrations via GMM and GMR

GMM and GMR are highly practical in learning and reproducing a human's desired behaviours from demonstration [7]. In this section, we will focus on how to teach the WMM the human's task-space behaviour for heavy object manipulation through HRC. Also, the null-space control for force exertion capacity enhancement is employed as presented in Section 4.3. Here, GMM is employed to encode the robot trajectory in the demonstration phase. In the lifting and lowering steps, the trained GMM and stiffness estimation technique are used to learn the demonstrator's impedance-based behavior; and in the carrying step, the trained GMM and GMR are adopted to

Algorithm 2 Personalization phase for mobility assistance via cooperative DMPs. (x motion as an example)

Prerequisite: Learned approximated f_{demo}; gait velocity $\dot{m}_{ave}$; η; δ; user's forces f_x and f_z; desired admittance parameters Υ_{x0}, Λ_{x0}, α, Υ_{xz}, and Λ_{xz}.

Steps:

Initialize two switch factors $\Delta_1 = 0$ and $\Delta_2 = 0$;
if $f_z \geqslant -f_z^{lim}$ && $f_z \leqslant -f_z^{in}$ && $f_x \leqslant f_x^{lim}$ **then**
    $\Delta_1 = 1$, $\dot{g}(\dot{x}_f) = \dot{m}_{ave} + \dot{x}_f$;
else
    $\Delta_1 = 0$, $\dot{g}(\dot{x}_f) = 0$;
end if
if $f_z < -f_z^{lim} \parallel f_x > f_x^{lim}$ **then**
    $\Delta_2 = 1$, $\dot{g}(\dot{x}_f) = 0$, calculate A via (18) with $m_L = g(\dot{x}_f) + \delta_g$ (δ_g is a small positive number);
else
    $\Delta_2 = 0$;
end if
Personalize user's motion using $\tau\dot{n} = \alpha_n(\beta_n(g(\dot{x}_f) - m) - n) + \Delta_1 f(\kappa) + \Delta_2 \delta\dot{A}$ and (16)-(18);
Activate the walker via (2) with $\dot{m}$ being the input $\dot{x}$.

encode and reproduce the WMM position trajectory taught by the demonstrator.

6.1. Gaussian Mixture Model for Data Encoding

During the demonstration phase, the WMM and the demonstrator are holding one end of the heavy object. The WMM is made compliant via the admittance controller and completely controlled by the demonstrator. The other end of the object is grasped by the coagent to achieve the task. All recorded data are divided into three portions corresponding to the three steps. For each step, each demonstration $l \in \{1, 2, \cdots, L\}$ consists of $T_{i,l}$ data points creating a dataset of N_i data points $\{\xi_{i,n}\}_{n=1}^{N_i}$ with $N_i = \sum_{l=1}^{L} T_{i,l}$, where L represents the number of the demonstrations and $i = 1, 2, 3$ denotes the manipulation step. Each $\xi_{i,n} \in \mathbb{R}^D$ is associated with the recorded data, including the end-effector position, velocity, and external force with D denoting the data point dimensionality.

Based on the demonstrations, the GMM is implemented to encode the data, presenting a probabilistic representation of the dynamics required to achieve the task. A GMM of $N_{k,i}$ components is expressed by a probability density function

$$p(\xi_{i,n}) = \sum_{k=1}^{N_{k,i}} p(k)p(\xi_{i,n}|k) \tag{23}$$

with $p(k) = \pi_{i,k}$ being the priors and $p(\xi_{i,n}|k)$ being the conditional density functions. In which, $\{\pi_{i,k}, \mu_{i,k}, \Sigma_{i,k}\}$ represent the parameters of the k^{th} Gaussian component of the i^{th} step, denoting the prior probabilities, mean vectors, and covariance matrices, respectively.

The optimal estimation of the mixture parameters is carried out iteratively implementing the Expectation-Maximization (EM) algorithm until convergence [43] and k-means procedure is used to initialize the model parameters. For the k^{th} Gaussian component of the i^{th} step, the E-step (expectation step) is expressed as

$$w_{i,n,k} = \frac{\pi_{i,k}\mathcal{N}(\xi_{i,n}|\mu_{i,k}, \Sigma_{i,k})}{\sum_k^{N_{k,i}} \pi_{i,k}\mathcal{N}(\xi_{i,n}|\mu_{i,k}, \Sigma_{i,k})}, \tag{24}$$

which plays an important role in deriving the stiffness of the virtual springs.

6.2. Demonstrator's Impedance-Based Behavior Learning in Lifting and Lowering Steps

During the lifting and lowering steps of the task, the human and the robot should exert a sizable force to neutralize the object's weight in the vertical direction. Here, we utilize several virtual spring models associated with each Gaussian component k to simulate the impedance-based behavior exerted by the demonstrator, which is expressed as

$$f_{s,i,n} = \sum_{k=1}^{N_{k,i}} w_{i,n,k}[K_{i,k}(\mu_{i,k}^x - x_{i,n})], \tag{25}$$

where $i = 1, 3$ indicates the lifting and lowering steps, $f_{s,i,n}$ is the demonstrator's force at step n, $K_{i,k}$ is a stiffness constant affiliated with the k^{th} Gaussian model, $\mu_{i,k}^x$ represents the positional component of the models' mean vectors $\mu_{i,k}$, and $x_{i,n}$ denotes the current end-effector position at step n.

Estimating the model stiffness in this paper is performed by implementing Least Squares (LS) estimation. After encoding the demonstration data via GMM, the observation matrix is defined as $\Phi_i = [\phi_{i,1}, \phi_{i,2}, \cdots, \phi_{i,N_i}]^{\mathrm{T}}$ with $\phi_{i,n} = [w_{i,n,1}(\mu_{i,1}^x - x_{i,n}), w_{i,n,2}(\mu_{i,2}^x - x_{i,n}), \cdots, w_{i,n,N_{k,i}}(\mu_{i,N_{k,i}}^x - x_{i,n})]$ using (24), and the demonstrator's force vector is denoted as $F_{s,i} = [f_{s,i,1}, f_{s,i,2}, \cdots, f_{s,i,N_i}]^{\mathrm{T}}$. Then, the unknown stiffness vector $K_i = [K_{i,1}, K_{i,2}, \cdots, K_{i,N_{k,i}}]^{\mathrm{T}}$ for all $N_{k,i}$ Gaussian models of the i^{th} step can be expressed as

$$K_i = (\Phi_i^{\mathrm{T}}\Phi_i)^{-1}\Phi_i^{\mathrm{T}}F_{s,i}. \tag{26}$$

Combined with (26), during the reproduction phase, the estimated demonstrator's force $f_{est,i,n}$ can be generated using (25) with the current end-effector's position.

6.3. Gaussian Mixture Regression for Trajectory Learning in the Carrying Step

During the carrying step, the heavy object will be moved in the horizontal plane to the predefined destination, and no extra force is required in the plane. Thus, only the kinematic model will be learned and reproduced using the demonstrations. With the GMM representation in Section 6.1, the reproduction of the movement in the horizontal plane can be formulated as a regression problem using GMR [12]. The GMR model can retrieve the next actions on-the-fly relying on the Gaussian conditioning theorem and linear combination properties of Gaussian distributions.

In conventional GMR, the query points are defined as temporal values ξ_t, and the corresponding spatial values $\hat{\xi}_s$ can then be estimated via regression. For the k^{th} Gaussian

component in the GMM of the second step, the mean vector and covariance matrix with consideration of input and output parameters are expressed as [44]

$$\mu_{2,k} = \{\mu_{2,t,k}, \mu_{2,s,k}\},\ \Sigma_{2,k} = \begin{pmatrix} \Sigma_{2,t,k} & \Sigma_{2,ts,k} \\ \Sigma_{2,st,k} & \Sigma_{2,s,k} \end{pmatrix}, \tag{27}$$

respectively.

In this step, the query points are defined as the time-independent end-effector positions, and the corresponding estimated parameters are the end-effector velocities. Thus, the demonstrator's behavior can be effectively imitated. The block diagram of the control system for object manipulation is illustrated in Fig. 4.

7. Experimental Setup and Results

Several experiments were conducted to demonstrate the effectiveness of the proposed approach. These included (A) the verification of the mobility assistance approach with the user intention taken into consideration, and (B) the validation of the human-robot collaboration for object manipulation using the LfD approach.

7.1. Experimental Setup

The experimental setup contained an omnidirectional WMM, an Axia80-ZC22 F/T sensor (ATI Industrial Automation, Apex, NC, USA), and a task-dependent end-effector. The WMM comprised a custom-built mobile platform and a 7-DOF ultra-lightweight robotic arm Kinova Gen3 (Kinova Robotics, Canada). An F/T sensor was employed to obtain the user's force and the object weight exerted on the WMM during the mobility assistance experiment and the HRC experiment, respectively. Two different end-effectors were designed for the proposed tasks. Fig. 5 shows the WMM prototypes, where an end-effector with two handles was provided (Fig. 5a) to assist the user, and a horizontal attachment was used (Fig. 5b) to fasten the WMM and the object to be manipulated.

The task-space dimension of the WMM in HRC was defined to be $r = 6$, considering both the position and orientation of the end-effector; however, only position compliance was treated. For the orientation, a simple PD controller was employed to maintain the end-effector's orientation constant. The joint torque limit vector was defined as $\tau_{m\,\mathrm{lim}} = [40, 40, 40, 40, 16, 16, 16]^{\mathrm{T}}$ Nm for the manipulator.

A video is attached with the manuscript to present the experiments in this section.

7.2. Mobility Assistance with a WMM

Mobility assistance is an important component in supporting the users' independent living. As shown in Fig. 1, only the mobile platform needed to be controlled to assist the user for mobility assistance; thus, we selected the weighting matrix in $J^{\dagger}$ of (2) as $W = \mathrm{diag}(I_{4\times4}, 0_{7\times7})$ to distribute no motion to the manipulator (meaning the configuration of the manipulator is constant as presupposed).

VAC is a practical method to detect the user's walking intention, which is realized by applying a force in the direction that the user wants to move. In previous research studies, only the horizontal forces were considered in the control of robotic systems for mobility assistance. Here, the vertical force was also taken into account to recognize the user's intention; specifically, a large vertical force demanded a small horizontal velocity. The following experiments in this section compare the performance of this new control method with the conventional VAC approach, which only employs horizontal forces. The participant in this experiment was a Ph.D. candidate (29 years old, male, 173 cm, and 69 kg) who attempted to walk in a manner that resembled the walking pattern of an older adult.

For this purpose, the admittance parameters implemented in the experiments were set as $\Lambda_{x0} = 75\,\mathrm{Ns^2/m}$, $\Upsilon_{x0} = 150\,\mathrm{Ns/m}$, $\alpha = 2\,\mathrm{s/m}$, $\Lambda_{xz} = 100\,\mathrm{Ns^2/m}$ and $\Upsilon_{xz} = 200\,\mathrm{Ns/m}$ using a trial-and-error method by optimizing the transient response and enhancing user's comfort in pushing the walker. These parameters may not be optimal but they are practical; if one wants to derive the optimal admittance parameters, the well-known linear quadratic regulator (LQR) can be applied [45]. It should be noted that the G_{xz} term in (4) is excluded in the traditional VAC approach by neglecting the vertical force. The experimental results for the applied forces and generated trajectories are shown in Fig. 6. With the conventional variable admittance controller, the horizontal motion was only dominated by the horizontal force (f_x). However, using the proposed method, the horizontal motion was also affected by the vertical force (f_z). When a larger vertical force was exerted at about 9.8 s in Fig. 6a, the resultant horizontal motion became slower due to G_{xz}. As shown in Fig. 6b, the tilt angle of the trajectory before 9.8 s was noted as θ_a and after 9.8 s was θ_b. With $\theta_a > \theta_b$, the speed of the smart walker was decreased. This performance of the proposed method is expected to be more suitable for older users who usually need the velocity to reduce substantially when a large vertical force is exerted to support their body weight.

The performance of the proposed cooperative DMPs in realizing mobility assistance during human bipedal walking, including emergency treatment for older users was tested. During the learning phase, the walker was launched via admittance control with small inertial and damping parameters ($\Lambda_x = 40\,\mathrm{Ns^2/m}$ and $\Upsilon_x = 80\,\mathrm{Ns/m}$) to be compliant enough for the user, allowing us to obtain the user's normal walking information. Three demonstrated trajectories were collected to attain sufficient gait information for the training system to learn the walking pattern in one gait cycle. The control parameters used in the experiments are listed in Table 1, which include both the learning and personalization parameters.

Fig. 7 shows the demonstrated trajectories (Fig. 7a) and the pre-processed walking gait data for walking pattern learning (Fig. 7b). As shown in Fig. 7b, five walking gaits were collected for human walking pattern personalization, where the gait period $T_{demo} = 2.25$ s and the average gait velocity $\dot{m}_{ave} = 0.1741$ m/s. The learned stride (shown in red dotted line) indicates the preferable learning performance of the DMP-based approach.

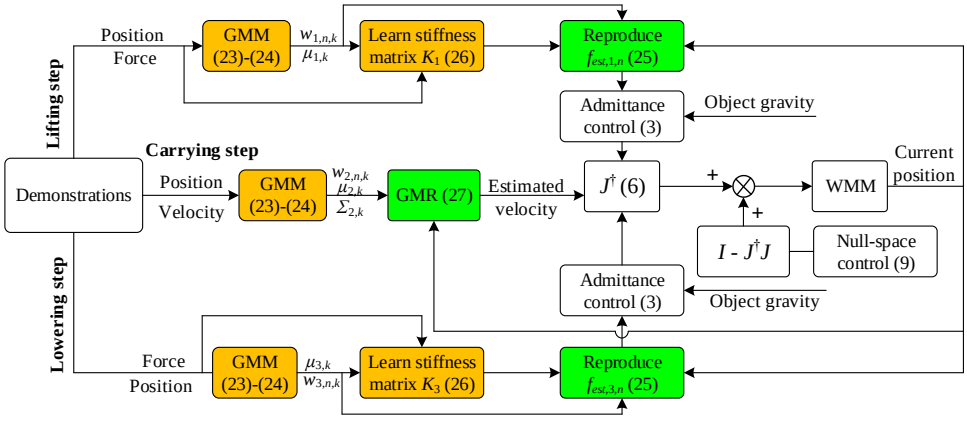

Figure 4: Block diagram of the object manipulation control system. The golden blocks denote the training system and the green blocks represent the reproduction system.

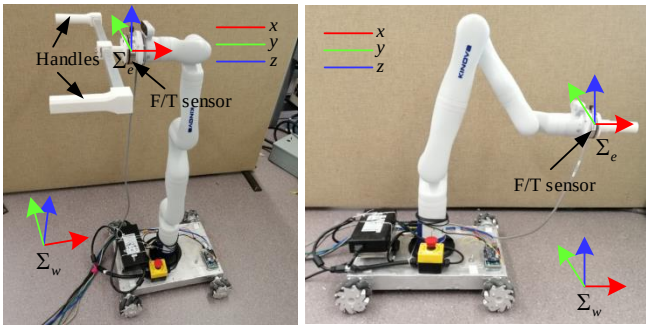

(a) Mobility assistance (b) Human-robot collaboration

Figure 5: WMM prototypes during the two experiments. Σ_e denotes the orientation of the end-effector, which is also the frame for the F/T sensor.

Table 1: Control parameters in the mobility assistance experiments.

Parameter	Value	Parameter	Value
N	12	τ	1
α_n (s^{-1})	4	β_n (s^{-1})	1
α_κ	0.05	η	10^4
δ	3	δ_g (m)	0.01
δ_t (s)	0.01		

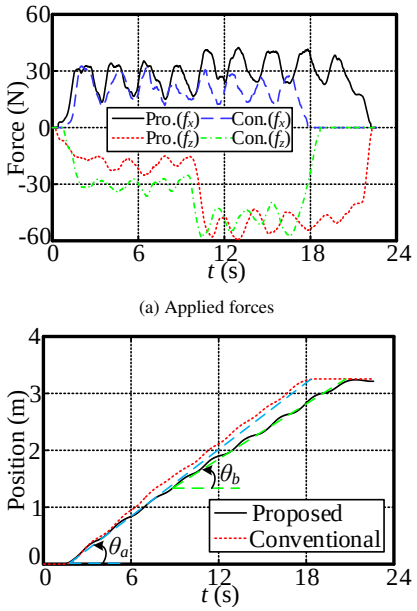

(a) Applied forces

(b) Resultant trajectories

Figure 6: Applied forces and resultant trajectories with the proposed method and the conventional method.

In the personalization phase, the walker followed the combination of the learned trajectory (realized by $\dot{m}_{ave}$) and the generated trajectory in terms of the interaction force (achieved by $\dot{x}_f$) based on **Step** 3 of **Algorithm** 2. The user's motion intention detection and emergency handling method were achieved using the wrist F/T sensor for user applied forces.

This process was able to provide walking pattern personalization and user intention adaptation simultaneously. As shown in Fig. 8, the actual motion of the walker behaved as though it was pulled by two springs whose origins are located on two different trajectories (generated by $\dot{m}_{ave}$ and $\dot{x}_f$). Snapshots of this experiment during walking are shown in Fig. 9. Fig. 10 compares the experimental results of (1) implementing only the proposed variable admittance controller and (2) using the cooperative DMPs. As shown in Fig. 10a, the walker moved approximately 3.2 m with almost the same speed via the two methods. The average traction force required for the VAC method was 17.9 N, while this force was reduced to 7.6 N by using cooperative DMPs, or 57.5%. This is because the DMPs model generated the control signal automatically when the human's walking intention was detected. From the right side of Fig. 10b, the maximum exerted power of the VAC method and the cooperative DMPs was 5.63 W and 2.59 W, respectively, resulting in a 54% improvement. The work exerted by the user during the two conditions was calculated as the integral of the applied power, $\int_0^t p_x \, d\tau$, which was 69.8 J and 24.4 J, respectively, also indicating the desirable performance of the cooperative DMPs in terms of saving user's energy.

Finally, the performance of the cooperative DMPs in han-

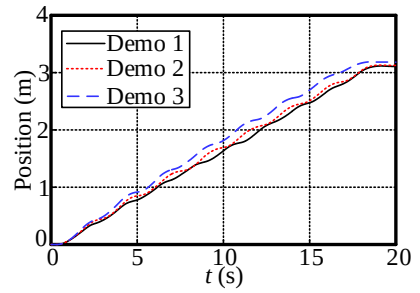

(a) Demonstrated trajectories

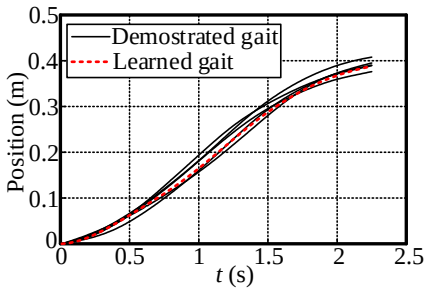

(b) Walking gaits

Figure 7: Demonstrated walking trajectories and walking gaits.

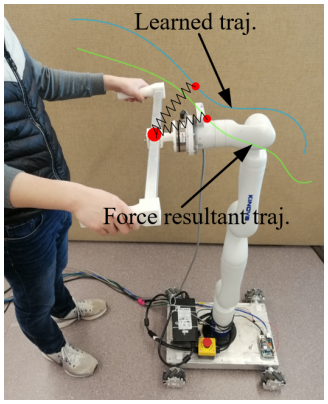

Figure 8: Illustration of the cooperative DMPs in the personalization phase.

dling an emergency was tested and the results are shown in Fig. 11. As stated earlier, a user may accidentally apply a large force, possibly caused by a probability of falling. This danger could be avoided by our strategy using (18). Meanwhile, the walker would not be activated if no force was detected using the circumvention term (17). The force thresholds of the participant were obtained by conducting some experimental tests. Here, the force thresholds in **Algorithm** 2 are set as $f_z^{lim} = 40$ N, $f_z^{in} = 5$ N, and $f_x^{lim} = 40$ N. As illustrated in Fig. 11, the user moved about 3.24 m. When a large vertical force (approximately 52 N) was applied at 8.03 s, the walker stopped ($\Delta_2 = 1$) with a reaction time no longer than 150 ms. The walker also gradually stopped at 18 s and 27.54 s after the user stopped applying any force ($\Delta_1 = 0$).

When the user stopped applying forces to the system, the walker still moved about 10 cm. This phenomenon resulted from the tracking error between the dynamic target $g(\dot{x}_f)$ and the actual walker position. Large control parameters α_n and β_n can reduce this tracking error but will cause unsatisfactory learning performance. However, the fast stoppage of the walker is realized when an emergency happens by adopting the additional term A in (15), (16), and (18), presented in Section 5.1.

7.3. Human-Robot Collaboration for Heavy Object Manipulation

Some heavy objects are unable to be lifted by a robotic system due to its limited joint torque output. With the implementation of a WMM, its redundancy can augment the system's force exertion capability in the vertical direction. It is noteworthy that this procedure is only for the null-space control to obtain an optimal WMM configuration (without changing the end-effector pose).

The control parameters in this experiment were set as $W = I_{11\times11}$, $W_\tau = \text{diag}(1, 1, 1, 1, 2.5, 2.5, 2.5)$, $k_N = 0.07$, $u = [0, 0, 1]^{\mathrm{T}}$, $\varrho = 600$, $w_1 = 0.6$, and $w_2 = 0.4$. The evolution of the WMM configuration is shown in the attached video, and the initial and final WMM configurations are shown in Fig. 12. The optimal WMM configuration for augmenting its load-carrying capability is shown in Fig. 12b. This is similar to how humans change their configuration to resist disturbance from the vertical direction.

The load-carrying ability of the WMM was compared in the two configurations that are depicted in Fig. 12 by adding known payloads to its end-effector. The results are shown in Fig. 13. During the experiment, first, a payload of 1 kg was added; and then, a weight of 3 kg was applied. Fig. 13a shows the manipulator joint torque output with the initial WMM configuration. When the 1 kg payload was added during time 5.40 – 21.05 s, all the joints could normally work with the maximal joint torque output being 35.31 Nm (joint 2). However, when the 3 kg weight was applied at time 31.38 s, the task stopped at 32.5 s due to the saturation of joint 2.

The joint torque output with the final WMM configuration is shown in Fig. 13b. With the 1 kg weight added during time 3.35 – 22.25 s, the joint with maximal torque output was joint 2, and the output was 26.24 Nm. When the payload of 3 kg was applied during time 34.70 – 54.90 s, the WMM with this configuration could also hold it, with the maximal joint output being 37.22 Nm (joint 2).

The joint torque increment caused by the end-effector force was investigated with a definition of weighted joint torque $\|\tau_{mw}\|_2 = \sqrt{\frac{\sum_{i=1}^{7} W_{\tau_i} \tau_{e_i}^2}{\sum_{i=1}^{7} W_{\tau_i}}}$, where W_{τ_i} denotes the i^{th} diagonal element of W_τ and τ_{e_i} represents the torque of the i^{th} manipulator joint caused by the external force. When the payload of 1 kg was applied, the weighted joint torque was reduced from 1.182 Nm to 0.869 Nm, about 26.5% of its previous value. With the 3 kg weight added on the WMM with the final configuration, the weighted joint torque was 2.559 Nm. These experimental results verified the effectiveness of the proposed method in augmenting the force exertion ability of the end-effector.

The final WMM configuration in Fig. 12b was employed to conduct the object manipulation task using HRC, and the

(a) (b) (c)

Figure 9: Snapshots of walking pattern personalization experiment. (a) initial state, (b) mobility assistance with the walker, and (c) final state.

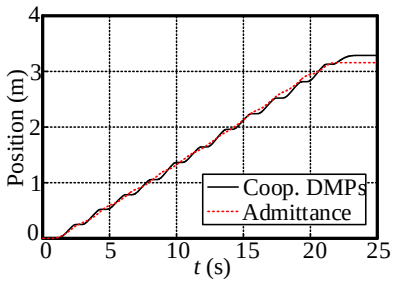

(a) Walking trajectories

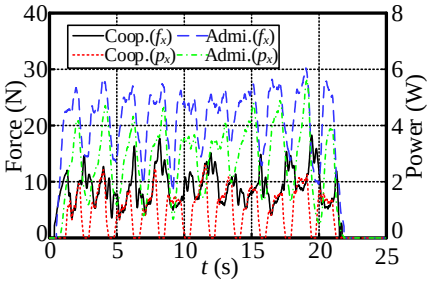

(b) Exerted forces and powers

Figure 10: Walking trajectories and exerted forces and powers during the experiments.

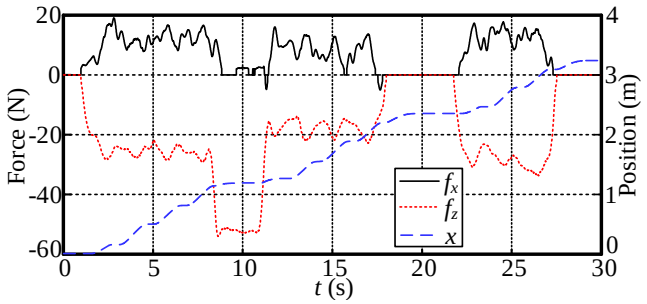

Figure 11: Performance of the cooperative DMPs in handling an emergency.

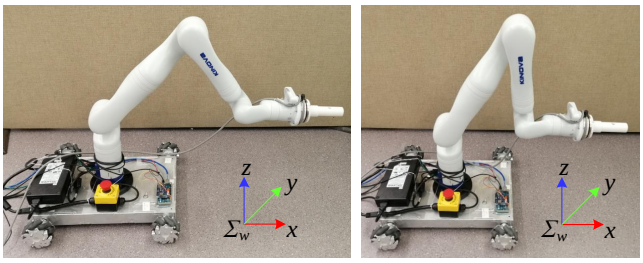

(a) Initial configuration (b) Final configuration

Figure 12: Initial and final WMM configurations with null-space control.

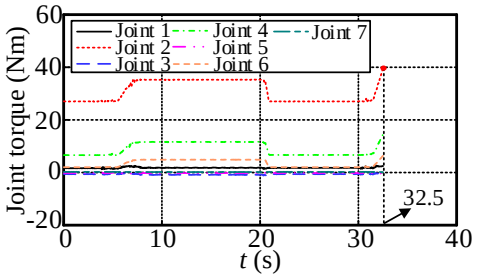

(a) Initial configuration

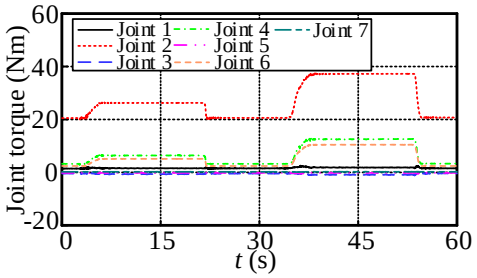

(b) Final configuration

Figure 13: Manipulator joint torque with two configurations.

null-space control was utilized. We selected three objects with weights of 1 kg, 3 kg, and 5 kg to demonstrate the performance of the LfD method in object manipulation. Two participants were involved to simulate the collaboration of two older adults, one human demonstrator (healthy, 29 years old, male, 173 cm, and 69 kg) and one human user (healthy, 34 years old, 176 cm, and 67 kg).

During the demonstration phase, the WMM was admittance-controlled to follow the human demonstrator to complete the object manipulation task with the user. The desired Cartesian impedance parameters for the WMM system were defined as $\Lambda = \mathrm{diag}(100, 100, 200)\,\mathrm{Ns}^2/\mathrm{m}$, $\Psi = \mathrm{diag}(200, 200, 400)\,\mathrm{Ns/m}$, and $\Gamma = \mathrm{diag}(0, 0, 0)\,\mathrm{N/m}$. The desired Cartesian impedance parameter Γ was set as zero to ensure that the robotic system could be led by the demonstrator smoothly.

For each object, four demonstrations were conducted, and snapshots of the demonstration phase are shown in Figs. 14a. The object's mass could be changed by adding or removing known payloads to simulate manipulating different objects.

The WMM trajectory and demonstrator's force in the ver-

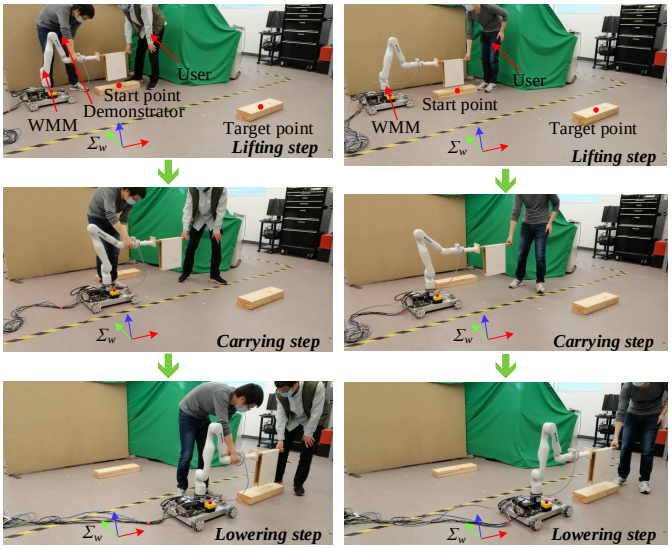

(a) Demonstration phase (b) Reproduction phase

Figure 14: Snapshots of demonstration and reproduction phases for object manipulation via HRC.

tical direction in the 5 kg scenario are shown in Fig. 15 to illustrate the performance of the proposed method. During the demonstrations, the average motion distances of the WMM in $[x, y, z]$ were $[0.908, -1.395, 0.167]$ m, $[0.978, -1.412, 0.165]$ m, and $[1.013, -1.412, 0.157]$ m for 1 kg, 3 kg, and 5 kg payloads, where the corresponding stable support forces were approximately 4.92 N, 12.32 N, and 18.39 N, respectively.

Then, we manually divided each demonstration data into three steps: lifting, carrying, and lowering to perform data encoding using GMM. Three models of ten components ($N_{k,1} = 10$), twelve components ($N_{k,2} = 12$), and ten components ($N_{k,3} = 10$) were selected to train the three steps with the obtained demonstrations.

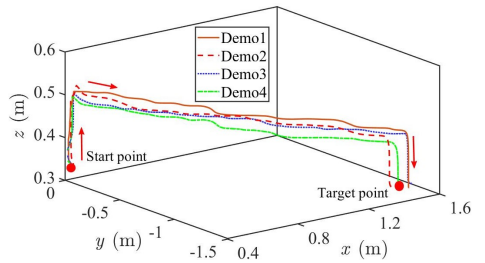

(a) Demonstrated 3D trajectory

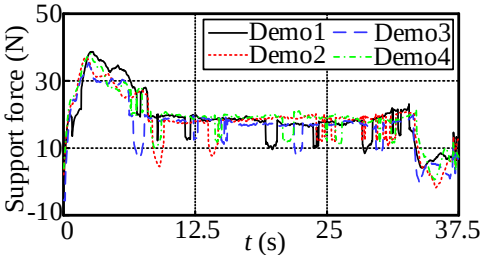

(b) Support force

Figure 15: Human demonstration for object manipulation with a 5 kg payload.

Fig. 16 shows the learning results for the lifting and lowering steps of the 1 kg load. In the lifting step (Fig. 16a), the demonstrator force was large enough to help the WMM lift the object with the user, while in the lowering step (Fig. 16b), the force was smaller due to object gravity. The *bottom row* of Fig. 16 presents the corresponding weighting matrices, which play an essential role in imitating the demonstrator's impedance in the reproduction phase. The learned models of the x axis and y axis in the carrying step of the 1 kg load are presented in Fig. 17, where the trained center and covariance matrix of each Gaussian model were employed to derive the end-effector's velocity according to its corresponding position via GMR.

In the reproduction phase, the WMM cooperated with the user to conduct the object manipulation task using the learned demonstrator's skills. Here, the admittance control was only implemented in the vertical direction during the lifting and lowering steps. The moment for step switching was detected when the end-effector reached the corresponding targets, or the number of iterations outstretched the demonstration samples' length. Some snapshots of the reproduction procedure are presented in Fig. 14b.

According to the demonstration data, we defined the motion target for the lifting and lowering steps as 16 cm, and for the x and y in the carrying step as 0.9 m and -1.35 m, respectively, in all three scenarios. The end-effector trajectories for the reproduction experiment are shown in Fig. 18. The learning results of the demonstrator's impedance in the lifting and lowering steps are presented in Fig. 19, and the position-velocity profiles (resulting from GMR) for x and y in the carrying step are provided in Fig. 20.

Fig. 18 shows that in the reproduction phase, the WMM can cooperate with the user to conduct the object manipulation task. In scenarios of 1 kg and 3 kg, the object could be lifted 16 cm as we expected, and the desired horizontal displacement in x reached 0.9 m. However, the displacement in y only arrived at 1.26 m and 1.31 m for l kg and 3 kg payloads, respectively. In the scenario of 5 kg, the motion displacements in x and z were 0.848 m and 15.6 cm, but the destination in y was reached. The reason for the inability to reach the destination in all three directions is the tolerance of the learning approach. In order to ensure accessibility, the algorithm should be modified to include some limitations, or the destination may need to be redesigned.

The reproduction results of the demonstrator's force and the horizontal velocity in Figs. 19 and 20 are similar to the results in the demonstration phase. The maximum of the mean absolute error (MAE) for the reproduced demonstrator's force relative to the mean of the demonstrated forces appeared in the lifting step of the 5 kg scenario, which was about 2.84 N, accounting for 8.35% of the maximal support force. The maximal MAE for the reproduced horizontal velocity was approximately 0.57 cm/s in the x direction in the 1 kg scenario, representing 12.1% of the maximal commanded velocity in the corresponding direction. Both the WMM trajectory and the reproduction results illustrate the effectiveness of the proposed method in helping a user perform object manipulation tasks.

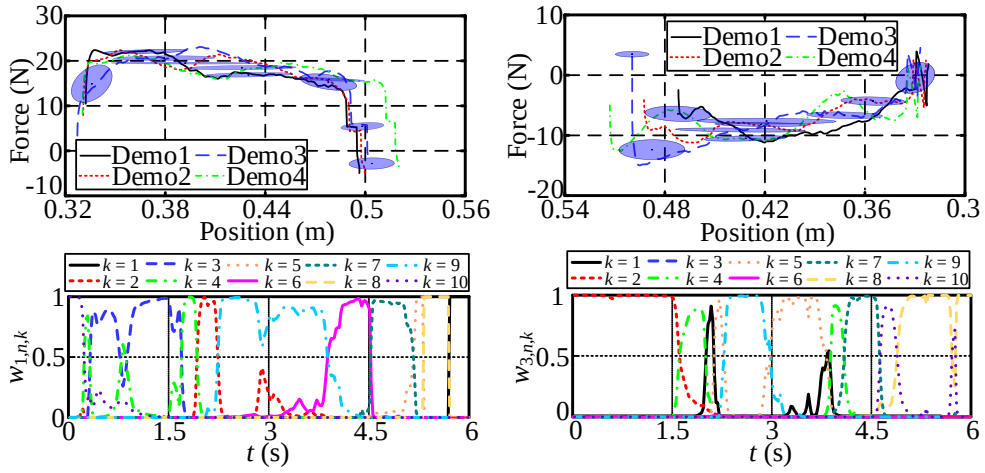

(a) Lifting step

(b) Lowering step

Figure 16: Model learning for lifting and lowering steps in 1 kg scenario. *Top row* shows the learned GMM and *bottom row* presents the corresponding model weights for demonstrator's impedance imitation.

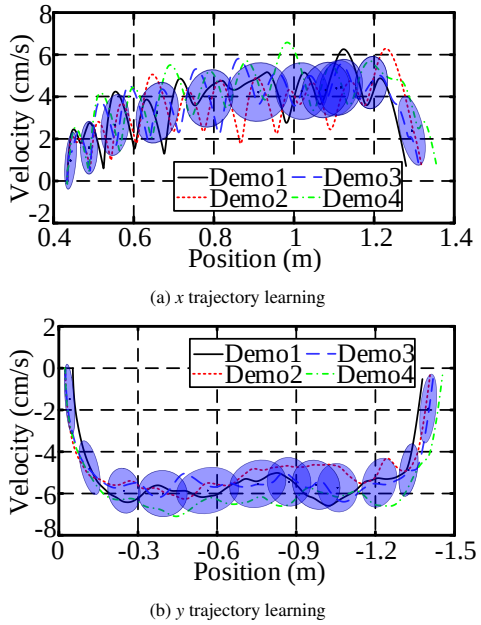

(a) x trajectory learning

(b) y trajectory learning

Figure 17: Model learning for carrying step in 1 kg scenario.

8. Conclusions

This paper developed an intelligent assistance device with a wheeled mobile manipulator (WMM) to tackle multiple tasks via task-dependent end-effectors. Two central challenges have been considered: mobility assistance and heavy object manipulation.

In mobility assistance, the user's walking intention was identified using a variable admittance controller, which interpreted the vertical and horizontal user-applied force components. Cooperative DMPs were implemented to learn the user's walking pattern over one gait cycle. The learned motion trajectory was then cloned for the next cycle to reduce the user's driving force while motion variations were adapted. Moreover, emergencies could also be avoided by having an additional coupled term in the cooperative DMPs.

In terms of heavy object manipulation, an HRC approach via LfD was proposed. The redundancy of the WMM was employed to enhance its end-effector's force exertion ability along the vertical direction to facilitate the carrying and transport of heavy objects. The entire procedure of this task was divided into three steps: lifting, carrying and lowering. GMM and a stiffness estimation technique were adopted to learn the demonstrator's impedance behavior in the lifting and lowering steps. GMM and GMR were implemented to reproduce the WMM motion in the carrying step.

The effectiveness of the proposed approach was experimentally verified. In terms of mobility assistance, the user would save up to 54% of their power and 65% of their energy to walk the same distance with the proposed strategy. The performance of the emergency handling method was successfully verified with a reaction time of less than 150 ms. For heavy object manipulation, the required weighted joint torque of the WMM for a 1 kg payload was reduced by 26.5% using the null-space control-based force exertion capacity enhancement method. Three loads with different masses were manipulated via LfD, and in terms of target point tracking, the experimental results showed that the reproduction error was no more than 7% of the desired value. While no user study was conducted, the technical validation confirmed the effectiveness of the proposed approaches.

Our future work will focus on three aspects. The first is integrating new sensory information (*e.g.*, leg and foot positions) for more accurate user intention detection. The second is designing automatic exchange devices for the task-dependent end-effectors to facilitate the user. And the third is employing online learning methods (*e.g.*, reinforcement learning) to reduce the tracking error for time-varying trajectories.

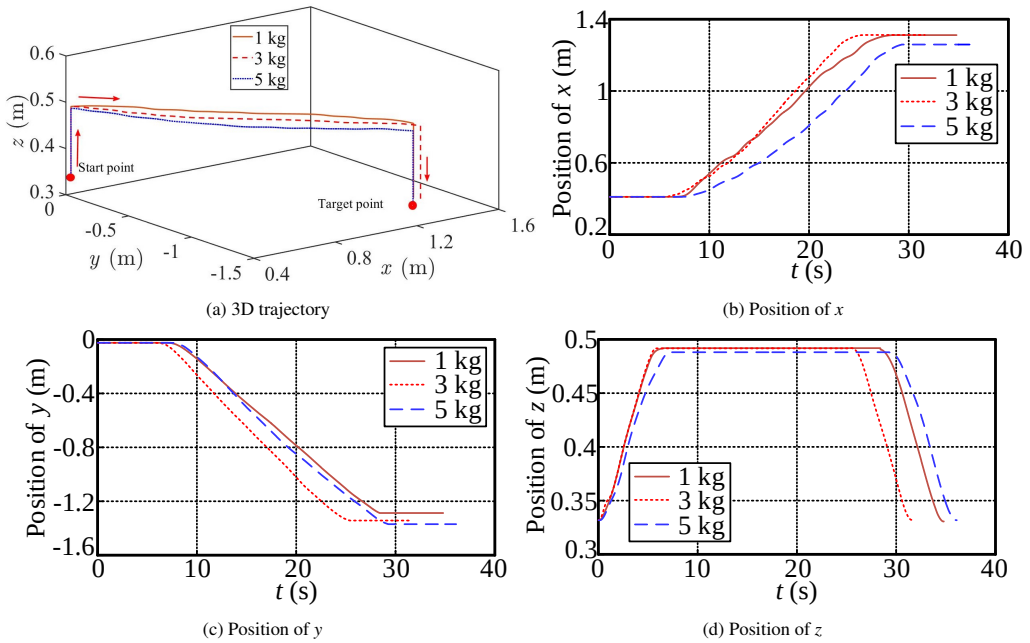

(a) 3D trajectory

(b) Position of x

(c) Position of y

(d) Position of z

Figure 18: End-effector trajectory in the reproduction phase.

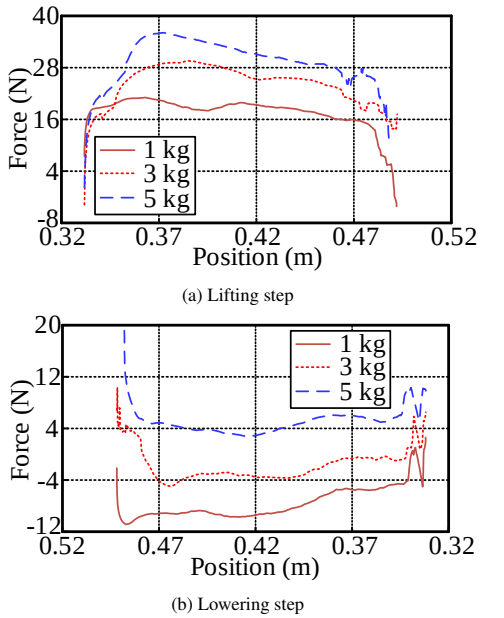

(a) Lifting step

(b) Lowering step

Figure 19: Reproduction results of the demonstrator's impedance-based behavior.

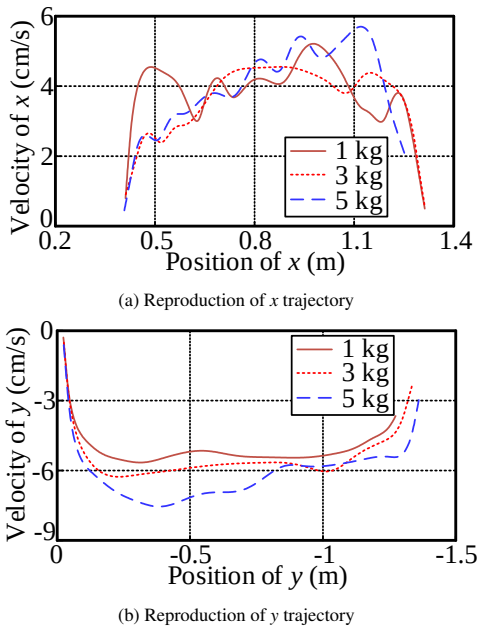

(a) Reproduction of x trajectory

(b) Reproduction of y trajectory

Figure 20: Reproduction of the horizontal trajectory in the carrying step using GMR.

Acknowledgements

This research was supported by the Canada Foundation for Innovation (CFI), the Natural Sciences and Engineering Research Council (NSERC) of Canada, the Canadian Institutes of Health Research (CIHR), the Alberta Jobs, Economy and Innovation Ministry's Major Initiatives Fund to the Center for Autonomous Systems in Strengthening Future Communities, the National Natural Science Foundation of China (Grant No. 91948202, 51822502), the "111" Project (Grant No. B07018), and the China Scholarship Council under Grant [2019]06120165.

References

[1] M. Martins, C. Santos, A. Frizera, R. Ceres, A review of the functionalities of smart walkers, Medical engineering & physics 37 (10) (2015) 917–928.

[2] H. M. Do, M. Pham, W. Sheng, D. Yang, M. Liu, Rish: A robot-integrated smart home for elderly care, Robotics and Autonomous Systems 101 (2018) 74–92.

[3] P. Xu, L. Ding, Z. Wang, H. Gao, R. Zhou, Z. Gong, G. Liu, Contact sequence planning for hexapod robots in sparse foothold environment based on monte-carlo tree, IEEE Robotics and Automation Letters 7 (2) (2022) 826–833.

[4] H. Xing, K. Xia, L. Ding, H. Gao, G. Liu, Z. Deng, Unknown geometrical constraints estimation and trajectory planning for robotic door-opening task with visual teleoperation assists, Assembly Automation 39 (3) (2019) 479–488.

[5] S. Itadera, E. Dean-Leon, J. Nakanishi, Y. Hasegawa, G. Cheng, Predictive optimization of assistive force in admittance control-based physical interaction for robotic gait assistance, IEEE Robotics and Automation Letters 4 (4) (2019) 3609–3616.

[6] H. Xing, A. Torabi, L. Ding, H. Gao, Z. Deng, V. K. Mushahwar, M. Tavakoli, An admittance-controlled wheeled mobile manipulator for mobility assistance: Human–robot interaction estimation and redundancy resolution for enhanced force exertion ability, Mechatronics 74 (2021) 102497.

[7] J. Fong, C. Martinez, M. Tavakoli, Ways to learn a therapist's patient-specific intervention: Robotics-vs telerobotics-mediated hands-on teaching, in: IEEE International Conference on Robotics and Automation, 2019, pp. 870–876.

[8] M. Tavakoli, J. Carriere, A. Torabi, Robotics, smart wearable technologies, and autonomous intelligent systems for healthcare during the COVID-19 pandemic: An analysis of the state of the art and future vision, Advanced Intelligent Systems 2 (7) (2020) 2000071.

[9] J. Fong, H. Rouhani, M. Tavakoli, A therapist-taught robotic system for assistance during gait therapy targeting foot drop, IEEE Robotics and Automation Letters 4 (2) (2019) 407–413.

[10] R. P. Joshi, T. Shibata, K. Ogata, Y. Matsumoto, Quantitative evaluation of clothing assistance using whole-body robotic simulator of the elderly, in: IEEE International Conference on Robot and Human Interactive Communication (RO-MAN), 2019, pp. 1–6.

[11] C. Moro, G. Nejat, A. Mihailidis, Learning and personalizing socially assistive robot behaviors to aid with activities of daily living, ACM Transactions on Human-Robot Interaction (THRI) 7 (2) (2018) 1–25.

[12] L. Rozo, S. Calinon, D. G. Caldwell, P. Jimenez, C. Torras, Learning physical collaborative robot behaviors from human demonstrations, IEEE Transactions on Robotics 32 (3) (2016) 513–527.

[13] A. Mörtl, M. Lawitzky, A. Kucukyilmaz, M. Sezgin, C. Basdogan, S. Hirche, The role of roles: Physical cooperation between humans and robots, The International Journal of Robotics Research 31 (13) (2012) 1656–1674.

[14] M. M. Martins, C. P. Santos, A. Frizera-Neto, R. Ceres, Assistive mobility devices focusing on smart walkers: Classification and review, Robotics and Autonomous Systems 60 (4) (2012) 548–562.

[15] Q. Yan, J. Huang, C. Tao, X. Chen, W. Xu, Intelligent mobile walking-aids: perception, control and safety, Advanced Robotics 34 (1) (2020) 2–18.

[16] H. Xing, L. Ding, H. Gao, W. Li, M. Tavakoli, Dual-user haptic teleoperation of complementary motions of a redundant wheeled mobile manipulator considering task priority, IEEE Transactions on Systems, Man, and Cybernetics: Systems (2022) 1–13.

[17] D. Ćehajić, S. Hirche, et al., Estimating unknown object dynamics in human-robot manipulation tasks, in: 2017 IEEE International Conference on Robotics and Automation (ICRA), IEEE, 2017, pp. 1730–1737.

[18] B. Navarro, A. Cherubini, A. Fonte, G. Poisson, P. Fraisse, A framework for intuitive collaboration with a mobile manipulator, in: 2017 IEEE/RSJ International Conference on Intelligent Robots and Systems (IROS), IEEE, 2017, pp. 6293–6298.

[19] H. Xing, A. Torabi, L. Ding, H. Gao, Z. Deng, M. Tavakoli, Enhancement of force exertion capability of a mobile manipulator by kinematic reconfiguration, IEEE Robotics and Automation Letters 5 (4) (2020) 5842–5849.

[20] C. Yang, C. Chen, W. He, R. Cui, Z. Li, Robot learning system based on adaptive neural control and dynamic movement primitives, IEEE Transactions on Neural Networks and Learning Systems 30 (3) (2018) 777–787.

[21] A. J. Ijspeert, J. Nakanishi, H. Hoffmann, P. Pastor, S. Schaal, Dynamical movement primitives: learning attractor models for motor behaviors, Neural Computation 25 (2) (2013) 328–373.

[22] J. Li, Z. Li, X. Li, Y. Feng, Y. Hu, B. Xu, Skill learning strategy based on dynamic motion primitives for human–robot cooperative manipulation, IEEE Transactions on Cognitive and Developmental Systems 13 (1) (2020) 105–117.

[23] O. Chuy, Y. Hirata, Z. Wang, K. Kosuge, Approach in assisting a sit-to-stand movement using robotic walking support system, in: IEEE/RSJ International Conference on Intelligent Robots and Systems, IEEE, 2006, pp. 4343–4348.

[24] M. Hu, Y. Chen, G. Zhai, Z. Gao, L. Fan, An overview of assistive devices for blind and visually impaired people, International Journal of Robotics and Automation 34 (5) (2019) 580–598.

[25] H. Yu, M. Spenko, S. Dubowsky, An adaptive shared control system for an intelligent mobility aid for the elderly, Autonomous Robots 15 (1) (2003) 53–66.

[26] R. Pérez-Rodríguez, P. A. Moreno-Sánchez, M. Valdés-Aragonés, M. Oviedo-Briones, S. Divan, N. García-Grossocordón, L. Rodríguez-Mañas, Friwalk robotic walker: usability, acceptance and ux evaluation after a pilot study in a real environment, Disability and Rehabilitation: Assistive Technology (2019).

[27] F. Ferrari, S. Divan, C. Guerrero, F. Zenatti, R. Guidolin, L. Palopoli, D. Fontanelli, Human–robot interaction analysis for a smart walker for elderly: The acanto interactive guidance system, International Journal of Social Robotics 12 (2) (2020) 479–492.

[28] M. Andreetto, S. Divan, D. Fontanelli, L. Palopoli, Path following with authority sharing between humans and passive robotic walkers equipped with low-cost actuators, IEEE Robotics and Automation Letters 2 (4) (2017) 2271–2278.

[29] M. F. Jiménez, M. Monllor, A. Frizera, T. Bastos, F. Roberti, R. Carelli, Admittance controller with spatial modulation for assisted locomotion using a smart walker, Journal of Intelligent & Robotic Systems 94 (3) (2019) 621–637.

[30] J. Fong, M. Tavakoli, Kinesthetic teaching of a therapist's behavior to a rehabilitation robot, in: IEEE International Symposium on Medical Robotics, 2018, pp. 1–6.

[31] A. Al-Yacoub, Y. Zhao, W. Eaton, Y. Goh, N. Lohse, Improving human robot collaboration through force/torque based learning for object manipulation, Robotics and Computer-Integrated Manufacturing 69 (2021) 102111.

[32] M. Gienger, D. Ruiken, T. Bates, M. Regaieg, M. MeiBner, J. Kober, P. Seiwald, A.-C. Hildebrandt, Human-robot cooperative object manipulation with contact changes, in: IEEE/RSJ International Conference on Intelligent Robots and Systems, IEEE, 2018, pp. 1354–1360.

[33] V. Villani, F. Pini, F. Leali, C. Secchi, Survey on human–robot collaboration in industrial settings: Safety, intuitive interfaces and applications, Mechatronics 55 (2018) 248–266.

[34] U. E. Ogenyi, J. Liu, C. Yang, Z. Ju, H. Liu, Physical human–robot collaboration: Robotic systems, learning methods, collaborative strategies, sensors, and actuators, IEEE Transactions on Cybernetics 51 (4) (2021) 1888–1901.

[35] H. Admoni, A. Dragan, S. S. Srinivasa, B. Scassellati, Deliberate delays during robot-to-human handovers improve compliance with gaze communication, in: ACM/IEEE International Conference on Human-robot Interaction, 2014, pp. 49–56.

[36] M. Saveriano, F. J. Abu-Dakka, A. Kramberger, L. Peternel, Dynamic movement primitives in robotics: A tutorial survey, arXiv preprint arXiv:2102.03861 (2021).

[37] H. Xing, A. Torabi, L. Ding, H. Gao, W. Li, K. M. Mushahwar, M. Tavakoli, Human-robot collaboration for heavy object manipulation: Kinesthetic teaching of the role of wheeled mobile manipulator, in: IEEE/RSJ International Conference on Intelligent Robots and Systems, 2021, pp. 2939–2946.

[38] E. Gribovskaya, A. Kheddar, A. Billard, Motion learning and adaptive impedance for robot control during physical interaction with humans, in: IEEE International Conference on Robotics and Automation, 2011, pp. 4326–4332.

[39] G. Kang, H. S. Oh, J. K. Seo, U. Kim, H. R. Choi, Variable admittance control of robot manipulators based on human intention, IEEE/ASME Transactions on Mechatronics 24 (3) (2019) 1023–1032.

[40] A. Gams, A. J. Ijspeert, S. Schaal, J. Lenarčič, On-line learning and modulation of periodic movements with nonlinear dynamical systems, Autonomous robots 27 (1) (2009) 3–23.

[41] A. Gams, B. Nemec, A. J. Ijspeert, A. Ude, Coupling movement

primitives: Interaction with the environment and bimanual tasks, IEEE Transactions on Robotics 30 (4) (2014) 816–830.

[42] R. Samant, L. Behera, G. Pandey, Adaptive learning of dynamic movement primitives through demonstration, in: IEEE International Joint Conference on Neural Networks (IJCNN), 2016, pp. 1068–1075.

[43] L. Rozo Castañeda, S. Calinon, D. Caldwell, P. Jimenez Schlegl, C. Torras, Learning collaborative impedance-based robot behaviors, in: Proceedings of the twenty-seventh AAAI conference on artificial intelligence, 2013, pp. 1422–1428.

[44] S. Calinon, F. Guenter, A. Billard, On learning, representing, and generalizing a task in a humanoid robot, IEEE Transactions on Systems, Man, and Cybernetics, Part B (Cybernetics) 37 (2) (2007) 286–298.

[45] C. Yang, G. Peng, Y. Li, R. Cui, L. Cheng, Z. Li, Neural networks enhanced adaptive admittance control of optimized robot–environment interaction, IEEE Transactions on Cybernetics 49 (7) (2019) 2568–2579.